Image Enhancement of Weather Degraded Images Using Computer Vision Techniques

By

Ehsan Ullah

2011-NUST-MS PHD-MTS-35

MS-70

Submitted to the Department of Mechatronics Engineering in Fulfillment of the Requirements for the Degree of

MASTER OF SCIENCE

in

MECHATRONICS ENGINEERING

Thesis Supervisor

Prof. Dr Javaid Iqbal, Ph.D

College of Electrical & Mechanical Engineering

National University of Sciences & Technology

2013

FORM TH-4

National University of Sciences & Technology

MASTER THESIS WORK

We hereby recommend that the dissertation prepared under our supervision by

Ehsan Ullah, Registration No. 2011-NUST-MS PHD-MTS-35 of MS-70

Titled:

Image Enhancement of Weather Degraded Images Using Computer Vision Techniques

be accepted in partial fulfilment of the requirements for the award of

Master of Science in **Mechatronics Engineering** degree.

Examination Committee Members

1. Name: Dr. Rab Nawaz Chaudhry Signature: _____

2. Name: Dr. Umer Shahbaz Signature: _____

3. Name: Dr. Khurram Kamal Signature: _____

Supervisor's Name: Prof Dr. Javaid Iqbal Signature: _____
Date : _____

_____ _____
Head of Department Date

COUNTERSIGNED

Date: _____ _____
Dean / Principal

بِسْمِ اللَّهِ الرَّحْمَٰنِ الرَّحِيمِ

In the name of Allah, the most Beneficent and the most Merciful

DECLARATION

I hereby declare that I have developed this thesis entirely on the basis of my personal efforts under the sincere guidance of my supervisor Prof Dr. Javaid Iqbal and co-supervisor Dr. Rab Nawaz Chaudhry. All the sources used in this thesis have been cited and the contents of this thesis have not been plagiarized. No portion of the work presented in this thesis has been submitted in support of any application for any other degree of qualification to this or any other university or institute of learning.

_____

Ehsan Ullah

ACKNOWLEDGMENTS

Innumerable words of praise and thanks to Allah, the Almighty. Without His Will and Mercy, I would not have been able to accomplish this milestone of my academic career.

I would like to thank my advisors Prof Dr. Javaid Iqbal, Dr. Rab Nawaz Chaudhry who guided me in my research. I would also like to thank my guidance and evaluation committee members, Dr. Khurram Kamal and Dr. Umer Shahbaz, for their continuous support and encouragement.

DEDICATION

To,

Our beloved Prophet Muhammad (PBUH) and his prayer for seeking knowledge that is beneficial for all.

اَللَّهُمَّ إِنِّي أَسْأَلُكَ عِلْمًا نَافِعًا , وَ رِزْقًا طَيِّبًا ,
وَ عَمَلاً مُتَقَبَّلاً

O Allah! I ask You for knowledge that is of benefit, a good provision and deeds that will be accepted.

[Ibn Majah and others]

ABSTRACT

Environmental effects, mist, haze, fog, snow and rain considerably effect visibility. The poor quality weather-degraded images perpetually effects performance of automated surveillance and tracking systems. Images enhancement and retrieval has a wide range of application, such as tracking and surveillance systems, consumer electronics and autonomous robotics Systems. Such applications generally require computationally efficient algorithm for cost effectiveness. By studying visual manifestation of various weather conditions in images, the environmental characteristics can be modelled effectively. Water droplets present in atmosphere cause mist, fog and haze effects due to scattering of light as it propagates through these particles. Subsequently, chromatic effects of image scattering can be reversed for retrieval of image information. Scattering of light affects image contents in proportion to the depth of scene. Classical image enhancement procedures are not effective as these do not take into account depth of image. Various model based as well as computer vision based techniques to enhance quality of weather-degraded images are in vogue. Physical modelling approaches, although promising better results in terms of color fidelity and contrast are computationally very expensive. Computer vision based techniques are computationally efficient; however usually result in compromising important information. An optimum blend of these two techniques is generally considered efficient means for the desired solution. *Single image dehazing technique using dark channel prior* is an advance approach with computational advantage being of first order. This technique has been further refined in this thesis by further improving estimation of *Atmospheric Light* and optimizing *transmission* sensitivity of the model. Contrast of the restored images has been considerably improved vis-à-vis color fidelity further refined. Improved re-defined model provides even better control on restored image parameters and fine tuning of contrast and color fidelity of recovered images. Feature detection, cross correlation, image registration, matching and recognition improves as input image quality improves. Image dehazing is an added feature to latest Night Vision Devices which can even pay dividend if utilised as a pre-processing stage. Major application of *Automated single image dehazing* techniques also include pre-processing of UAVs, GIS, and satellite imagery, where it is not feasible to obtain same images again.

NOMENCLATURE

DC	Dark Channel
I(x)	Input image , hazy image
J(x)	Restored image, haze free image
t(x)	Transmission
β	Atmospheric coefficient
ʎ	Wavelength
μ	Frequency
L∞, A	Atmospheric Light
ρ (x)	Reflectance
w	Aerial prospective
t_0	Lower threshold of transmission
ϕ	Sensitivity control coefficient
RGB	Red green blue color channel

TABLE OF CONTENTS

LIST OF FIGURES

LIST OF TABLES

CHAPTER 1

INTRODUCTION

Classical computer vision system have inherent design to work in clear weather, however weather can cause a veil in the form of fog, mist, snow and rain. Image enhancement of weather degraded images is a unique interdisciplinary challenge, involving meteorology, optical physics as well as computer vision and computer graphics. Dominant weather factors like mist, haze and limit visual range in the atmosphere, as well as, reduce contrast in scenes. A main objective in such analysis is improvement of visibility and recovery of colors, as if imaging is done in clear conditions. Computer vision and human vision can then capitalize on such improved images for various applications, such as long range surveillance [..]." [Namer and Schechner, 2005]. Also, "In general, the haze-free image is more visually pleasuring. Second, most computer vision algorithms, from low-level image analysis to high-level object recognition, usually assume that the input image (after radiometric calibration) is the scene radiance.

Poor visibility and contrast are the main effects caused by the presence of water droplets present in the atmosphere. Light is scattered as it interacts with these particles in it course towards camera from scene. Besides scattering absorption and emission phenomenon also take place but scattering is the most pertinent to our application. Mist, fog and haze are categorised on the basis of size of particle which are in the range of 1-10 μ meter. Size of these particles is in close comparison with the wavelength of light. As concentration of water droplets increases in light path so amount of light reduces that directly reaches to camera, causing a decrease in intensity of light. On the other hand, more particles interact with light beam and concentration of scattering and polarization of light increases manifolds. Various weather conditions dependencies on atmospheric particle size and concentration has been tabulated in table 1.1.The performance of computer vision algorithms (*e.g.*, feature detection, filtering, and photometric analysis) will inevitably suffer from the biased, low-contrast scene radiance. Haze removal can improve performance of these algorithms. As a byproduct haze removal produces depth information and benefits many vision algorithms and advanced image editing. Haze or fog can be a useful depth clue for scene understanding.

Condition	Particle Type	Radius	Concentration
Air	Molecule	10^{-4}	10^{19}
Haze	Aerosol	10^{-2}	10^{3}-10
Fog	Water droplet	1-10	100-10
Cloud	Water droplet	1-10	100-10
Rain	Water drop	10^{-2} -10^{-4}	10^{-2}- 10^{-5}

Table 1.1 Weather Condition and Particles size [McCartney 1975]

The need for image enhancement stems from the fact that the atmosphere is never free of particles. With just pure air, the visual range has been found to be between 277km [Hulbert, 1941] to 348km [Middleton, 1952], not considering the curvature of the earth's surface. However, real visual ranges are much less than this theoretical value. The international visibility code for meteorological range rates visibilities between 50m up to over 50km for exceptionally clear air, visibility decreases as the scattering coefficient increases. Fog categorization based on density of scattering coefficient is described in table 1.2. These highway codes have been found to reflect a convenient scale for visual ranges in the daily work of meteorologists. The difficulty of image content retrieval becomes more difficult as the concentration of impurities increases. Depth of image also need to be estimated, the more accurate is depth approximation, the more sharp and enhanced is the quality of restored image.

Code	Fog Category	Visibility Range	Scattering Coefficient
1	Dense	< 50 m	> 78.2
2	Thick	50 - 200 m	78.2 -19.6
3	Moderate	200 – 500 m	19.6 – 7.82
4	Light	500 – 1000 m	7.8 – 3.9
5	Thin	1 – 2 Km	3.9 – 1.9
6	Haze	2 – 4 Km	1.9 -0.95
7	Light Haze	4 – 10 Km	0.95 – 0.39
8	Clear	10 – 20 Km	0.39 -0.19

Table 1.2 Visibility Range and Scattering of Atmospheric Particles [Hulbert,1941]

Computer Vision has been a very rapidly growing field over past few decades. Digital images interpretation enables autonomous robotics systems to perform their tasks more efficiently and promptly. However, outdoor navigation and surveillance mainly depends upon types of image input. Performance of such systems is adversely affected by the degradation of input images. Weather effects like, haze, rain, mist and fog provide a veil in-between scene and image. As a result, image quality is deteriorated which perpetually alter the desired output.

Although physics of image optics has research background spread over centuries, however image retrieval and restoration is still a challenging job for online tracking and navigation systems. Researchers have been working for restoration of environmental model and calculation of light scattering and attenuation. These methods required multiple images of same scene acquired at different times. Physical models promise better results but computationally very intensive. Image Enhancement techniques are under constraint problems as these utilize single image. These methods are based on various prior assumptions' and computationally efficient. Although results are not very precise, but provide a reasonable workable solution for real time systems.

1.1 Motivation

There has been a lot of research work in last two decades in fog removal / image dehazing using various approaches due to wide range of applications. The major application areas are listed as follows:

1. Aerial Imagery has a lot of application in navigation and tracking. In preprocessing stage, weather affects needs to be removed for better interpretation of imagery.
2. Outdoor Navigation and tracking system are based on input from digital cameras, due to fog and haze threshold values may be disturbed and system may not capture the desired response. Image pre-processing to remove fog / haze effect may be required for effective operation of such systems.
3. A wide Range of military application from target acquisition, tracking and capturing at preprocessing stage may enhance the performance of Night Vision Devices.

4. Under Water Imagery can be enhanced as utilizes similar model for propagation and scattering of light through a medium.
5. It has application in consumer electronics like digital cameras additional features.

1.2 Research Objectives

Weather effects has a wide spectrum of effects on images, however main focus of the research was on most dominating effects, which are mist, haze and fog. Following were the main objectives of the research work:

a. Study the human visual model and image interpretation by visual receptors
b. Effects of EM wavelength and frequency on weather parameters
c. Light transmission and scattering
d. Mathematical model of degraded images by fog
e. Effect of parameter of mathematical model
f. Previous work done in fog removal from images
g. Latest techniques of haze removal using single image
h. Selecting optimum dehazing algorithm and refinement in procedure

CHAPTER 2

VISION AND IMAGE THEORATICAL ANALAYSIS

'Those who wish to succeed must ask the right preliminary questions."

(Aristotle)

Image enhancement of weather degraded images requires a thorough understanding of basics of image formation methodology and it its attributes. There are some models which work on human vision model for retrieval of image contents.

2.1 Human Visual Perception

Computer vision applications are based on mathematics and probability, human perception of images still has pivotal role in application of the techniques. Developing an understanding of human perception of imagery parameters and comparison with machine perception pays rich dividends.

2.1.1 Eye Anatomy and Image Formation

The optical system of the eye is composed of three main components, cornea, iris, and the lens (Figure. 2.11).The structures of these three components are very complicated, discussion is limited to their optical properties. The anatomy of eye has been discussed only to the extent to which it impacts quality of image.

Cornea is the first surface which is an extension of the sclera. Sclera is a relatively tough, white in color and can be called the outer shell of the eye. The transparency of the cornea is attributed to the regular layers of fibers that comprise most of the corneal thickness. Periodic closures of the eyelid provide a thin tear film on the cornea's external surface, which provides a smooth refracting surface. The variations in the tear film cause scattering and small changes in optical aberrations.

The centre of cornea has about 0.5 to 0.6 mm thickness, a mean refractive index of about 1.376. Its first surface has a radius of curvature of about 7.7 mm, where as its back surface radius is about 6.8 mm. This attributes to cornea a total power of roughly 43 diopters. As the cornea contribute most of the power of the eye, so it is also a key donor for aberrations of the eye. The conic shape of cornea balances out it high magnitude of aberration which could be resulted in case of a spherical shape. Due to the minor flattening of the corneal curvature toward the periphery lowers further the amount of spherical aberration to about one-tenth of that in spherical lenses of similar power. In general variations in corneal shapes contribute to astigmatism and higher order aberrations.

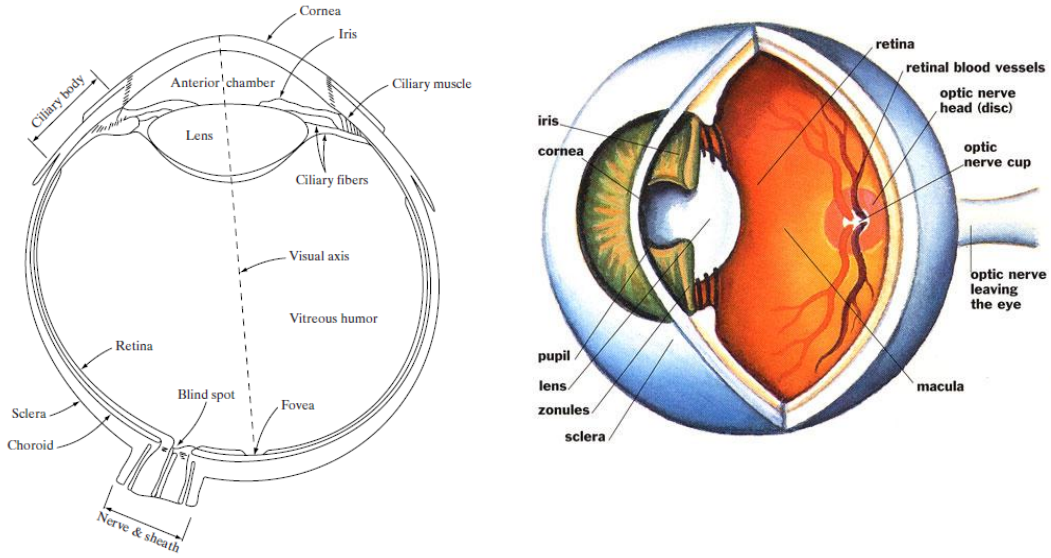

Figure 2.1: Structure of eye

The pupil in eye performs two main optical functions. Firstly limits the amount of light that reaches the retina, and secondly varies the size of aperture of the eye. Due to the aberrations in the eye, the biggest pupil may not always give the optimum image quality. Although the optimal pupil size is criterion dependent, but for visual spatial frequencies, the diameter of most favourable pupil size is 2-3 mm. Pupil is situated between the cornea and lens, it serves as an aperture stop, it means that field of view of eye is not changed by varying its size. This orientation of cornea limits off-axis aberrations and its size also provide the eye a field of view that covers almost the full hemisphere.

The lens is situated immediately behind the iris and contributes another 20–30 diopters to the optical system of the eye. It is held firmly in place near its equator via zonules which are attached to the ciliary body. The tension on the zonules is released by narrowing of the ciliary muscle. This mechanism increases lens curvatures and facilitates the eye to focus on closer objects. Similarly as tension on the zonules increases by relaxing the ciliary muscle, it causes flattening of the lens and allow eye to focus on far off objects. The capability of lens to change it shape reduces as it hardens with age.

Crystalline lens is made of manifold layers of long, lens fiber cells that stems from the equator and spread towards poles of the lens. Suture patterns are formed at the meeting point of the cells. Structure of lens continues evolution throughout life cycle, crystalline structure formation and growing of lens continues throughout the age cycles.

Due to development pattern of crystalline lens, it has a gradient refractive index. Gradient refractive index has been a very important research topic since its inception. Nature of exact gradient of eye is still unknown, but it has its peak value in the centre at about 1.415 and drops off first slowly and then quickly near the surface to 1.415 Refractive Index. This gradient may be attributed to design or natural properties of the biological tissues in the eyes, but it cannot be ignored.

Retina is the innermost membrane of the eye and it is the portion on which light is focused and image is formed. It has on its surface discrete receptors which support pattern vision. These receptors are extremely sensitive in nature and have very fast response. Receptors have been named, cones and rods. There are about 6 – 7 Million cones which are located on central portion of the retina. This central portion is highly sensitive to color and termed as fovea. These cones can resolve fine details in color as each is connected to its nerve end. The eyeball is rotated by the controlling muscles until the image of target object falls on the fovea. Cone vision is termed as bright vision or photopic vision. There are about 75-150 Million rods which are also spread on the surface of retina. Rods are distributed over a relatively larger area, however, several number of rods are attached to a single nerve end. These structural properties of rods reduce the amount of details translated by these receptors. Rods provide an overall picture of the field of view and are very sensitive to low level view of illumination. These are not involved in

color vision. As an example, colorful objects appear colorless under moonlight as only rods are activated in low light, phenomenon is referred as scotopic or dim-light vision. Same objects reflect color when seen in daylight as cones are activated.

Distribution of visual receptors rods and cones is measured in degree from the fovea. It is in degree off-axis. It is a measure of the angle formed by the visual axis and a line passing from the center of lens and intersecting retina. In Figure 2.2 density of rods and cones for right eye has been depicted. Visual receptors are distributed in radial symmetric pattern except for blind spots. Blind spots are areas where no receptors are present.

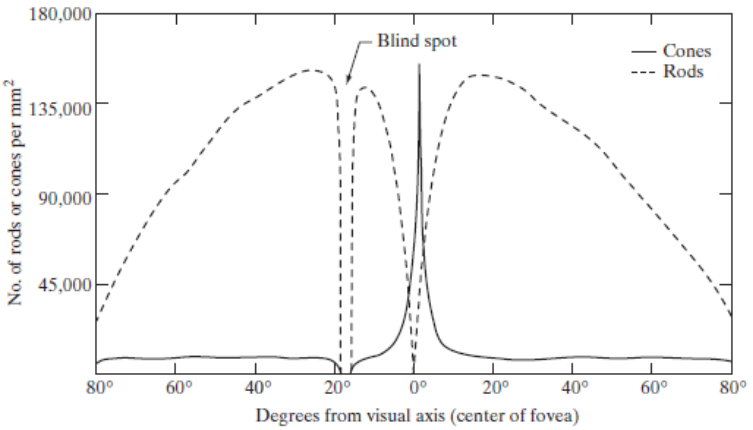

Figure 2.2: Distribution of Rods and Cones including Blind Spots

It is evident from Figure 2.2 that maximum density of cones is in the centre of the retina. On the other hand, density of rods increases from centre outwards to 20° off axis and decrease in density outwards on extreme periphery of retina. Note also that rods increase in density from the center out to approximately off axis and then decrease in density out to the extreme periphery of the retina.

Although fovea is a circular indentation of 1.5 mm in diameter in the retina, however in terms of image processing elements square or rectangular array are more practical. Therefore, we view fovea as square sensor array of dimensions 1.5 mm * 1.5 mm. In retina area, cones have a density of 150,000 elements per mm^2. As per above data, number of cones in highest acuity regions are in the range of 337,000 elements approximately. If we compare eye with charge

couple device in terms of raw resolving power, a CCD imaging chip of medium resolution would require an area of 5mm x 5 mm for earlier mention density of receptors. Human has the ability to integrate intelligence and experience with vision has no match with machine vision. The key factor to remember is that basic ability of eye to resolve detail is within realm of current imaging systems.

2.1.2 Image Formation in Eye

If we compare an optical lens and an eye lens, eye lens is more flexible. Referring to Figure 2.1 it is clear that curvature radius of the anterior lens surface is greater than the radius of its posterior surface. Eye lens shape is flexible and it can be controlled by the tension of cilliary body's fiber. Lens focusing muscle cause the lens to flatten for focusing distant elements and thickens to focus objects in close vicinity. The focal length of eye lens is the distance between the center of the lens and the retina. It ranges between 14-17 mm. Lens works on its minimum refractive power when eye focuses on an object farther away than about 3 m, the lens exhibits its lowest refractive power. Similarly eye lens work on maximum refractive mode, when it focuses on a nearby object. Size of retinal image can be computed based on this information. Figure 2.3 explains calculation of height of retinal image. A tree of 15 m is at a distance of 100m from observer, the geometry yields 15/100=17/h or h=2.55 mm. Image of object is formed on fovea of retina area, light receptors in the area transform this light energy into electrical energy signals which are finally processed by brain.

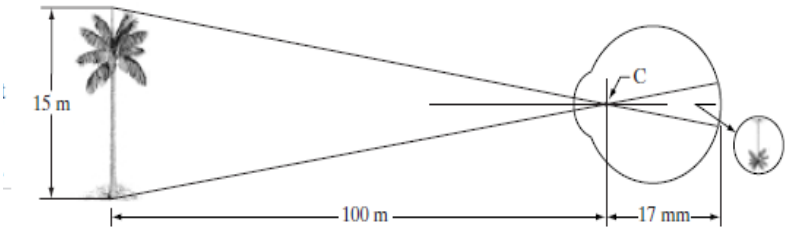

Figure 2.3: Image Formation on Retina

2.2 Intensity and Brightness Discrimination

Human eye has the ability to adapt to a very wide spectrum of light intensities. It is of the order $10^{10,}$ on the lower side it is in scotopic threshold while of higher level it includes glare. It has been verified by the experiments that brightness perceived by human brain is a logarithmic function of incident light on eye. In image processing digital images which includes discrete intensity levels over a range. Eye ability to discriminate between discrete levels is very critical. It is a logarithmic function of the light intensity incident on the eye. Figure 2.4, exhibits the relation between light intensity and subjective brightness.

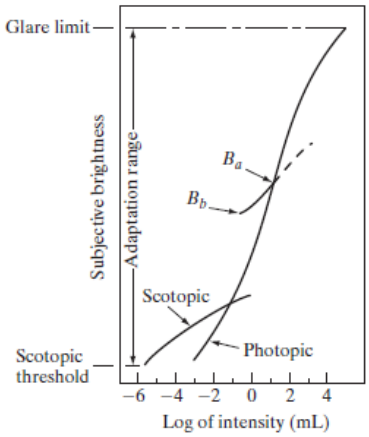

Figure 2.4: Intensity of Light and Human Eye Perception

The graph elucidates the range of intensities to which human visual receptors respond (represented by solid curve in graph of Figure 2.4). In the photonic vision the range is 106. There is a smooth transition from scotopic to photopic over the corresponding range from 0 .001 to 0.1 milli amber.

2.3 Response to Color

There are various types of cones for detecting various wavelengths. A specific cone has particular response sensitivity to a small interval of light wave length. The maximum of sensitivities are 419nm for the first type, 530nm and 558nm for the second and third type, respectively. For this reason, the cones are also classified by L (long), M (medium), and S (short) cones, referring to the wavelengths. With the information about the distribution of wavelengths over three sampling values our brain is able to conceive the light color. However, the cones need

a minimum light intensity in order to function, which lies at about the light intensity of bright moonlight or the sky light right after sunset, in numbers this corresponds to 10^{-2} cd $m^{-2.}$ As the light intensity falls underneath that threshold, the fourth kind of receptor, the rods, begin to surrogate the light detection. However completely switching from photopic vision (cones) to scotopic vision (rods) takes up to 30 minutes, this mechanism is called dark adaption.

The rods have a much lower response time, which allows humans to perceive higher speeds of objects and higher frequencies of light flare. Also the sensitivity of rods is much higher than that of cones. The maximum wave length sensitivity of rods lies at about 505nm (which corresponds to a color between green and blue). Because there is only one type of dark light receptor (one wavelength), colors cannot be perceived when the eye is dark adapted. This leads to the overall response of the human eye to wavelengths between 380nm to 760nm. Figure 2.2 shows the segment of wavelength where the eye has its maximum sensitivity. In this figure one curve represents the sensitivity for photonic vision, the other for scotopic vision.

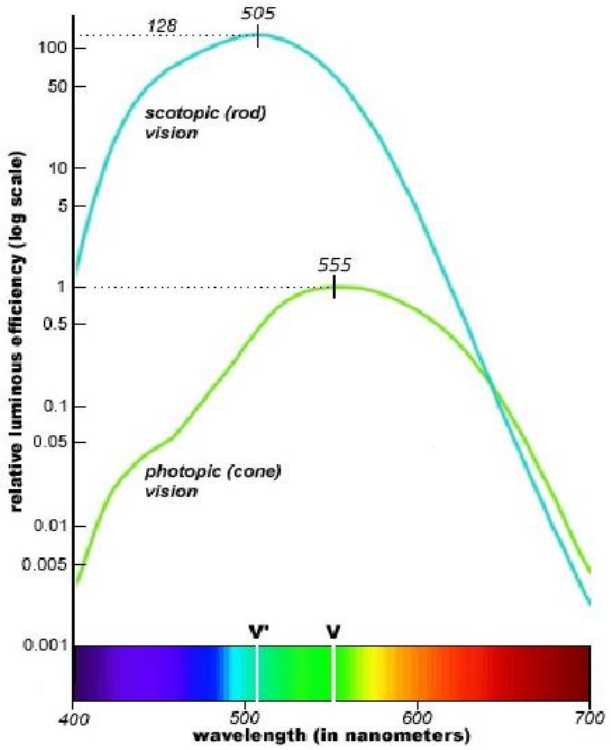

Figure 2.5 Rods and Cones Wavelength Response

Source: [Laserpointerforums.com, 2010]

2.4 Electromagnetic Spectrum and Light

Images in visible range of electromagnetic (EM) spectrum are more important than imaging in other neighboring bands. Newton discovered that when a beam of white light passes through a glass prism it is scattered into continuous spectrum of colors from violet at lower wave length end to red at higher wave length. Figure 2.6 illustrates that visible light consists of a very small portion of EM spectrum. Wave length of EM spectrum varies from km rages for Radio Waves to millions of times smaller for Gama rays on other end. EM spectrum
The relation between wavelength (λ) and frequency (μ) for the EM spectrum is expressed as:

$$\lambda = \frac{c}{\mu} \qquad (2.1)$$

Where c is the speed of light (2.998 x10^8 m / s). The Relation for energy of the electromagnetic spectrum is given as:

$$E = h\mu \qquad (2.2)$$

In equation 2.2, h is Planck's constant and wavelength is measured in meters. The appropriate units for EM spectrum are microns (denoted m and equal to 10^{-10} m) and nanometers (10^{-9} m). Frequency is measured in Hertz (Hz), and defined as number of cycles per second. Energy of various constituents is usually measured in electron-volt (e V).

Visible light is a portion of EM spectrum which can be sensed by human eye as illustrated in Figure 2.6. The wavelength of visible spectrum spread over from 0.43 to 0.79 x which gives colors: violet, blue, green, yellow, orange, and red. It is evident from Figure 2.6 that transition among different colors is not abrupt rather it is smooth. Perception of colors is attributed to the nature of light reflected by the object under observation. White color is due to the balanced reflectance of all colors. Similarly different shades of a color are due to reflectance of light with primarily in that color while absorbance of other colors. As an example green color shades are result of other energy wavelengths. An object appears black when it absorbs all visible color wavelengths.

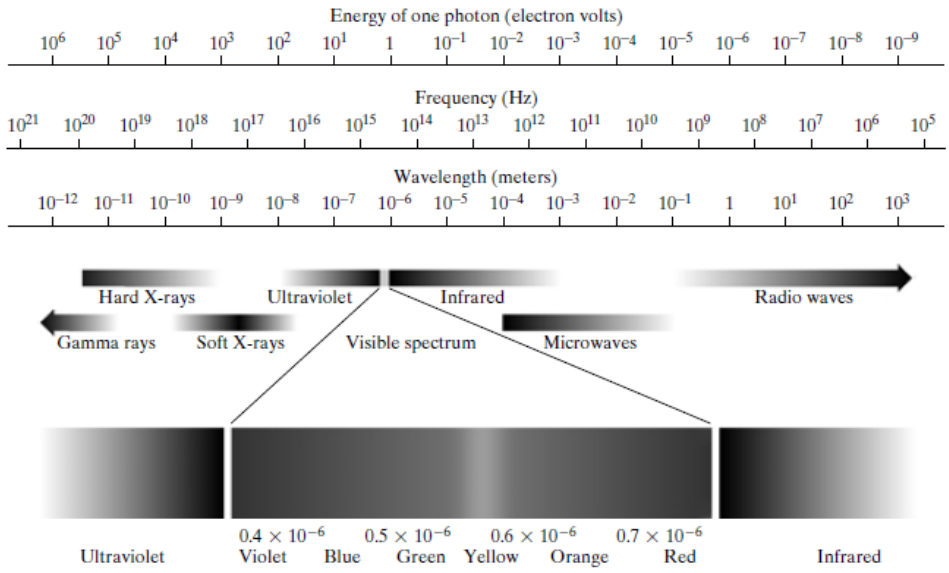

Figure 2.6: Energy, Frequency and Wavelength of EM Spectrum

Light which has no color component is called monochromatic light. Term gray level is used to mention such images and it includes various shades of gray, from black till white. Color or chromatic light has wavelength in the range of 0.43 – 0.79 x 10^{-6} m. The quality of color is estimated from three basic parameters which are radiance; luminance; and brightness. Radiance is measured in watts and defined as total amount of energy which emits from light source. Luminance is form of light energy which an observer perceives from light source. It is measured in lumens (lm). An infrared source of light has radiance but it luminance is zero, that is reason why it is not perceived by human eye. Brightness of an image cannot be measured as it is subjective to various environmental sources.

Wavelength of a source of energy is of vital importance as its interaction with the sensor helps in its detection and estimation. It is just like size of holes in a strainer which would capture specific elements. In case of an EM spectrum, for detecting a specific object, we must utilize the wavelength which is of same size or smaller than the object. If it is desired to detect a molecule of size in range of 10^{-10} m, accordingly a source must be utilized in far X rays, having equivalent wavelengths.

CHAPTER 3

LITERATURE REVIEW

3.1 Historical Prospective

Image enhancement in computer vision has it roots in Atmospheric Physics, which deals with light properties as it propagates and interacts with atmosphere. These include light propagation, interaction with water droplets in air, reflection, refraction and scattering. It also help to explain various visual phenomenon like blueness of sky, color of horizon and formation of rainbow [Minnaeart 1954 and Henderson 1977]. Literature and works in the fields of optics has a span period of over two centuries [Narasimhan & Nayar,2003]. Light changes it properties as it propagates through different denser air layers, its characteristics phenomenon like diffraction, scattering, absorption and emission, in a way code the information of atmosphere. If accurately demodulated, this information can be utilized for image restoration and enhancement by applying inverse function of degradation.

Atmosphere is a complex phenomenon and various assumptions are needed for modeling light scattering and propagation. Haze, mist and fog terms have been used synonymously for the degradation effect caused by the scattering of suspended particles varying in size 1-10 μm. Due to rapid boom in communication and imaging device, past two decade involve large volume of research and development work in ‘fog removal from images’ or ‘dehazing’. This also attributes to the dependence and boom of surveillance and tracking infrastructure and demand for automation and autonomous functionality. The research can be categorized into two broad segments:

a. Fog Removal using Image Enhancement Techniques
b. Fog Removal using Image Restoration Techniques

3.2 Enhancement Techniques

Classical image enhancement methods of image processing are based on assumption that light travels from scene element to camera in a transparent medium and medium depth has no role in enhancement of intensity and contrast. These methods treat fog as a impurity which has

distorted image intensity and contrast. Fog also drift color of the true image, these techniques fails to restore color fidelity of restored image. However, the restoration quality is subject to application and density of the fog. Popular enhancement based techniques includes , unsharp masking, retinex theory, and wavelet approaches

3.2.1 Histogram Techniques

Histogram is very easy to implement in intensity improvement techniques for clear images. Histogram techniques have been also crafted for fog removal and applicable to some specific problems where intensity improvement can work. Histogram equalization methods spread the intensity of input image over all levels based on the probability distribution of histograms. Global histogram equalization techniques are computationally less expansive, however do not improve small details of image. Local histogram equalization employs algorithm on small kernel and enhance minor details. This requires more calculations to be performed.

Many researchers tried to exploit histogram equalization technique for improvement of fog removal from images. Kaijun Zhu[Kaijun ,2006] used image segmentation for fogy image into flat area, image area where no variance exists, and non flat area. Histogram equalization of non flat area was done which provides good results for specific application.

Pei Zhu[Pei Zhu,2006] further tried to improved histogram equalization utility for sky area which usually include dense fog by applying normal distribution as per the grey area. Ping Wang [Ping, 2006] proposed a variant of local histogram equalization and blended it with PHOSE algorithm to maximize its efficiency. Although this method provided good image intensity but at the same time it added some blurring effect when image sub block was used.

Zhiyuan Xu[Zhiyuan,2008] proposed a histogram method for intensity enhancement based on Bilinear Interpolation Dynamic Histogram Equalization. Original image is first segmented into some segmented images, later histogram of each segment is divided into smaller parts. Then new dynamic ranges are to be allotted to new segments, finally bilinear interpolation and histogram equalization are administered for input image.

Histogram methods has an inherent limitation that it does not take into account depth of the scene, where as fogy image has distortion in proportion to the depth of the scene. This limitation provides a limited result as compared to model based techniques. Histogram implementation process pixel by pixel and in case of aerial images of high resolution, methods has practical limitation of huge processing.

3.3 Restoration Techniques

These methods provide relatively better results for fog removal as these include depth of the scene. Fog is due to presence of heavy concentration of suspended water droplets in the air, and their size is in comparison with wavelength of light. Scattering as a chain reaction adds a component of trapped light in image whereas intensity of the scene degrades exponentially as a function of distance. The model used to describe fogy image is:

$$I(x)= J(x)t(x) + A(1- t(x))$$

Here J(x) is haze free image, t(x) is transmission of light which reaches the camera and I(x) is fogy image. In case of homogeneous atmosphere t(x) is a function of depth dx and atmospheric coefficient (β) of the image.

$$t(x) = e^{- \beta dx}$$

It is evident from equation that depth estimation of image is essential for model based approach. Depth of image can be obtained using stereoscopic methods which require multiple images. Due to their limitation for real time systems later methods have been developed using single image and depth is estimated using various priors and assumptions.

3.3 Fog Removal using Multiple Images

3.3.1 Multiple Image using Polarization Filters

Earlier dehazing method focused on the basic of fog formation in the atmosphere which is due to chain reaction of suspended water droplets in air. Polarization of light due to light

scattering has been modeled by various light scattering models. This method usually uses two input images taken with two differently polarized filters, taken successively to produce one haze free image. Polarization method is based on the fact that the airlight is at least partially polarised, whereas the direct transmission of the object is not polarized. Polarization filters alone cannot eliminate haze in scenes, at least two images with different polarization filter states are necessary.

Figure 3.1 illustrates the working setup of the philosophy, camera receives two components from object, direct transmission is the component of light which is not scattered and reaches camera. Second component is scattered by the fog and partially polarised. Airlight is the partially polarised and algorithm transmission can be used for restoration of haze free image. Polarization filter with variable orientation is placed in front of the camera with variable angle α. Orientation at which image is least dense is corresponds to minimum value of airlight.

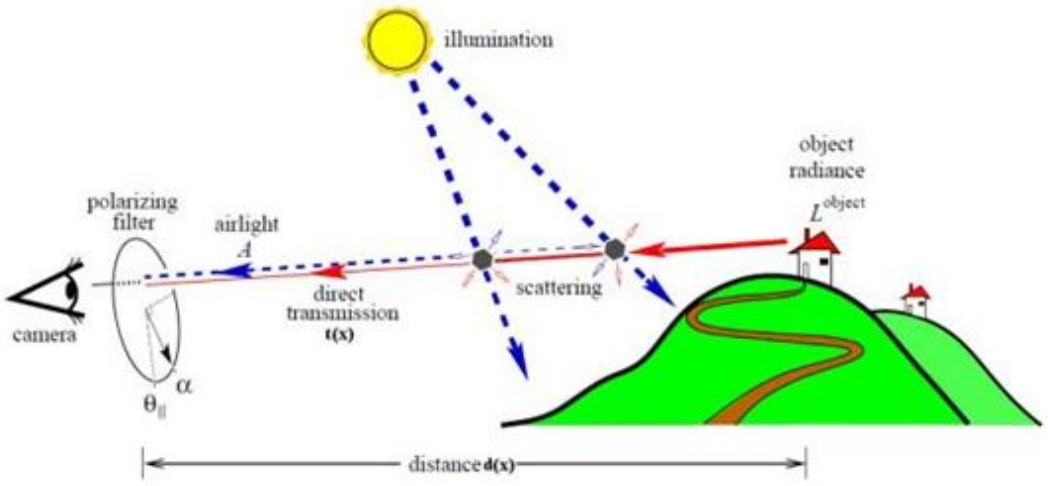

Figure: 3.1 Polarization Filter Based Dehazing

Image restoration of fogy image is good in terms of visibility and color fidelity, however it is cumbersome due to polarization filter sensitivity to weather conditions and orientations. It cannot be applied to a data set of images as require multiple images of different polarization. Image restoration example is shown in figure 3.2, two images with different level of polarization has been taken as input images and then repeated variation of polarization gives different result. Quality of output depends on the precision of polarization filter which is very sensitive to weather parameters.

Figure: 3.2 Image Restoration Using Polarization Filters.

There are other multiple image input techniques, like dehazing method of Nayar and Narasimhan as mentioned in their work [Nayar and Narasimhan, 1999] and [Narasimhan and Nayar, 2002], which take images under different fog densities and employ complex calculations, hence not feasible for real-time applications.

Oaklay [Oaklay1998] presented a physical model method which require prior information of the scene, like depth of the scene elements. It does not require weather information of the scene. This method has its limitation and fails when prior information is not provided by the user.

3.4 Single Image Dehazing

Due to complexity of multiple images and depth information dependence of the scene element, single image based restoration methods have been devised. Mathematically, dehazing using a single image is an under constraint problem as number of unknown are more than number of equations. The solution of under constraint problems is possible only using some

priors or assumptions. These methods use various priors' information for depth information and categorized in two classes:

3.4.1 Interactive Single Image Dehazing

Kopf et al presented a state of the art interactive methodology for dehazing which is named '*Deep Photo System'*. The core of the system is the accurate depth information of each pixel by a image registration method of existing state of the art navigations infrastructure. In present world of google earth, it can be assumed that 3D model of each scene can be borrowed and exact distance can be acquired from GPS system. It is foresighted to have better accuracy rather than relaying classical statistical priors and assumptions.

Exact distance and depth of the scene point can be calculated from 3d models of the cities from VirtulaEarthTM. It is important that the scene must be geo-referenced only once initially and could then rely on a set of depth information indefinitely assuming no camera shifts take place. Depth information of construction infrastructure is also available in maps and plans data. The system has its limitation as it cannot be applied to the scene for which no depth information is recorded. Also for moving cars and airplanes no depth information is available. It can be ignored if distances are very much and effect of movement is negligible.

Kopf et al. approximates the airlight and the attenuation factors in the same manner to the other haze removal methods and then basically solves Koschmieder's equation, however with some nuances differently. In the paper [Kopf et al., 2008], the authors explore further possible applications for the depth information of an image, other than dehazing, such as approximating changes in lighting, expanding field of view, adding haze, adding new objects into the image with the correct haze values according to distance, and integration of GIS data into the photo browser, just to name a few. Since often the depth map of other dehazing methods also comes as a byproduct, these mentioned applications may also be implemented combined with other dehazers, such as [Fattal, 2008] or [He et al., 2010a], for example. Problems may arise from the fact that the alignment between the photograph and the model may not be completely accurate due to imprecise 3D models or the lens curvature of the imaging system.

3.4.2 Automated Single Image Dehazing

Recent work propose single image dehazing using various prior about depth of the scene, these method are computationally efficient and suitable for real time systems.

3.4.2.1 Fattal's Method

Fattal proposed a very effective technique in 2008 based on single image dehazing that yielded qualitatively improved results on fogy images. The basic idea of this method is to take the image degradation model from Rossum and Nieuwenhuizen [Rossum and Nieuwenhuizen, 1999]) also known as the Radiative Transport Equation and translated in terms of surface shading in addition to the transmission. This results in an improved model of hazy image."This allows us to resolve ambiguities in the data by searching for a solution in which the resulting shading and transmission functions are locally statistically uncorrelated. A similar principle is used to estimate the color of the haze." [Fattal, 2008].

$$I(x) = t(x)J(x) + (1 - t(x))A$$

Where t(x) is transmission which is a scalar quantity for each color channel.

$$t(x) = e^{-\beta d(x)}$$

The model and variables are similar to the preceding sections. This equation is commonly used to describe the image formation in the presence of haze and was used before by, for example [Chavez, 1988], [Nayar and Narasimhan, 1999] and [Shwartz et al., 2006]. This inherits many ambiguities in each pixel independently, such as in the airlight-albedo, that gives a large degree of freedom. Fattal however, manages to reduce this degree: "To reduce the amount of this indeterminateness, we simplify the image locally by relating nearby pixels together." [Fattal, 2008]. He does that by grouping pixels belonging to the same surface, thus having the same surface reflectance and therefore the same constant surface albedo. Now the key idea to resolve the airlight-albedo ambiguity is that he assumes that the surface shading *l* and the scene transmission t are statistically uncorrelated, because *l* depends on the illumination on the scene,

surface reflectance properties and the scene geometry, whereas t depends on the density of the haze (β) and the scene depth. Fattal then presents an independent component analysis method to determine *l* and t. The same principle of correlation is applied to the estimation of the airlight color. This method also gives a depth map, which could be used over and over again for a static camera when using it in a real-time application. "The Method works quite well for haze, but has difficulty with scenes involving fog, as the magnitude of the surface reflectance is much smaller than that of the airlight when the fog is suitably thick." [Carr and Hartley, 2009]. According to Fattal, the noise level in the input image influences the quality of the dehazed image greatly. However, with Fattal's method the absolute error in transmission and haze-free image are both less than 7% in tests where the real haze free image was known, explanatory: "In its essence this method solves a non-linear inverse problem and therefore its performance greatly depends on the quality of the input data." [Fattal, 2008]. "Moreover, as the statistics is based on color information, it is invalid for grayscale images and difficult to handle dense haze which is often colorless and prone to noise." [He et al., 2010a].

3.4.2.2 Tan's Method

Tan presented a single image based dehazing method in 2008, too. His proposed method is based on the optical model:

$$I(x) = L\infty\, \rho(x) e^{-\beta d(x)} + L\infty(1 - e^{-\beta d(x)})$$

with $L\infty$ being the atmospheric light and $\rho(x)$ the reflectance, this formula is very similar to Koschmieder's equation . The first term in this equation is the direction attenuation and the second term corresponds to the airlight A. He then expresses it in terms of light chromaticity and as a vector for the color components. In this formula there are more unknowns than known's. Nevertheless, there are some clues or observations that Tan makes use of in his algorithm:

1. "The output image, [..] must have better contrast compared to the input image I." [Tan, 2008]
2. "The variation of the values of A[atmospheric light for the color components] is dependent solely on the depth of the objects, d, implying that objects with the

same depth will have the same value of A, regardless their reflectance(ρ). Thus, the values of A for neighboring pixels tend to be the same. Moreover, in many situations A changes smoothly across small local areas. Exception is for pixels at depth discontinuities, whose number is relatively small." [Tan, 2008]

3. "The input images that are plagued by bad weather are normally taken from out-door natural scenes. Therefore, the correct values of [the direct attenuation] must follow the characteristics of clear-day natural images." [Tan, 2008]

Tan algorithm can be implemented by following flow diagram as shown in figure 3.5.

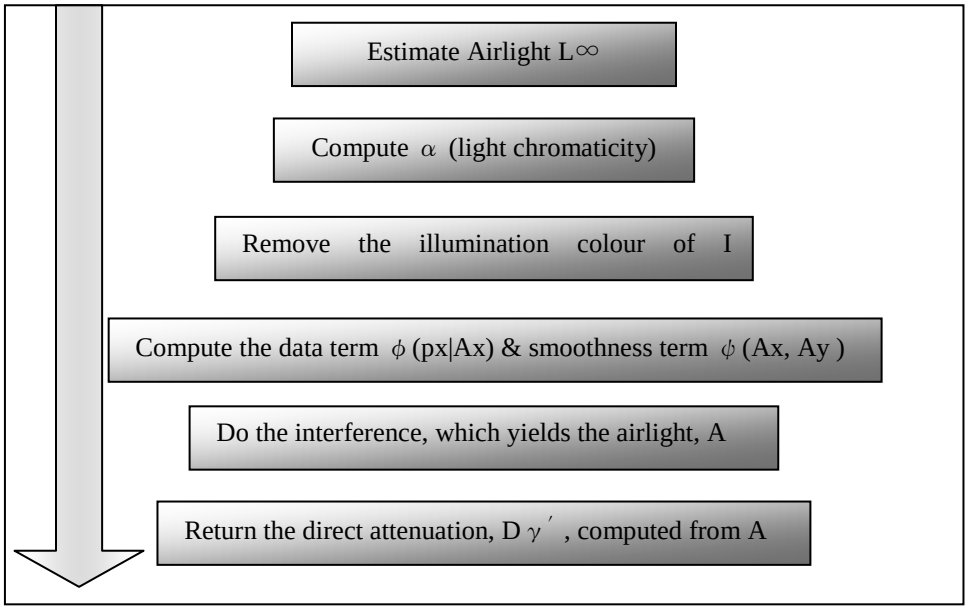

Figure 3.3 Tan's Method Flow Diagram

Fattal also proposed a cost function for estimation of data term in step 4 by employing Markov Random Fields which can be optimized by various procedures like graph-cuts. Although this optimization is valid for color as well as gray scale images but color images original color are not restored to desired fidelity level. Due to its computationally expensive nature it is not feasible for real time systems. "The computational time for 600x400images, using double processors of Pentium 4 and 1 GB memory, approximately five to seven minutes (applying

graph-cuts with multiple labels)" [Tan, 2008]. Moreover, there are some quality issues with this method compared to other methods, for example Fattal and Kopf et al. in terms of image quality. Since it produces halos near depth discontinuities and "The method tends to produce over enhanced images in practice." [Carr and Hartley, 2009].

Chronology of work on the domain of fog removal for the last two decades has been listed in table 3.1. This includes the most referred and valuable work, some of which like Dark Channel has been registered as a patent.

Table 3.1 Chronology of Restoration Based Fog Removal Methods **[Abhishek,2012]**

Method	Input Images	Assumptions	Image Type
Oakley et al. (1998)	Multiple	Knowledge of scene depth	Gray
Schenchner et al. (2001)	Multiple	Light scatters by atmospheric particles is partially polarized	Color and gray
Narasimhan et al (2002)	Multiple	Uniform bad weather condition	Color and gray
Narasimhan et al (2003)	Single	Interactive	Color and gray
Oakley et al. (2007)	Single	Airligth is constant throughout	Color and gray
Kim et al. (2008)	Single	Cost function of human visual model	Color
Kopf et al (2008)	Single	Interactive	Color and gray
Fattal (2008)	Single	Shading and transmission functions are locally uncorrelated	Color
He et al (2009 -12)	Single	Dark Channel prior	Color and gray
Tarael et al (2009)	Single	Assumes Airlight as a percentage between local standard deviation and local mean of whiteness	Color and gray
Zhang et al (2010)	Single	Under the assumption that large scale chromaticity variations are due to transmission while small scale luminance variations are due to scene Albedo	Color and gray
Fang et al (2010)	Single	Based on black body theory and black based image segmentation	Color and gray

CHAPTER 4

METHODOLOGY

'Single Image Dehazing using Dark Channel Prior with improved Atmospheric light estimation and optimum modelling to improve contrast and Intensity of restored images'

Image dehazing is a very challenging problem as it is an under constraint problem, Kaiming He proposed a novel method based on strong priors. Dark Channel is the prime assumption which is based on the observation that most haze free images has at least one color channel which has minimum intensity approaching to zero. Experimentations has confirmed that optimizing the model and estimating optimum values for a specific problem yields good results with improved contrast and color fidelity. The proposed method is also computationally efficient as computational complexity is of first order.

4.1 Dark Channel Prior

Satellite imagery has been prone to weather effects like fog, mist and rain and Dark Object Subtraction [Chavez 1988] suggested 'subtraction of a constant value proportion to the max effect'. Images histograms were used to estimate the intensity value require to be subtracted from the scene elements. However, haze is not uniform in majority of the cases and depends on the depth of the scene.

Statistical study of outdoor imagery revealed that most local regions of the images has at least one of the color (RGB) channel has very low intensity and it approaches to zero. However, in case of fog as light scattering effect in proportion to the depth of the scene ads Atmospheric light effect, hence minimum intensity of the dark channel of the hazy image is not zero. The channel which is estimated by minimum values of RGB is termed as Dark Channel. In hazy images, dark channel provides an estimation of the haze element present in the image. There are few exception to dark channel phenomenon and it becomes invalid when scene element are very similar to Atmospheric light, as an example a white wall over a large local region. Dark Channel provide a good solution for most of the outdoor haze images and for exceptionally white image

content over a white background, haze itself becomes invisible. The Figure 4.1 illustrates dark channel concept.

Figure 4.1: Dark Channel a: Haze free images b: Dark Channel of haze free c: Hazy Image and its Dark Channel

Histogram of haze free image and hazy image further tells the nature of image and its intensity value ranges.

Dark channel for an arbitrary image J, expressed as J^{dark} is defined as

$$J^{dark}(x) = \min_{y \in \Omega(x)} \left(\min_{C \in \{r,g,b\}} J^{C}(y) \right)$$

In this J^{c} is color image comprising of RBG components, $\Omega(x)$ represents a local patch which has its origin at x. The operation involves two min operator, $\min_{C \in \{r,g,b\}}$ is performed on each pixel and

picks min value of three RGB color channels. The second operator $\min_{y \in \Omega(x)}$ is a min filter of suitable window size which is performed on image. In mathematics, min operators are commutative in nature.

Observation of haze free images infers that dark channel of such images is very low and approaches to zero:

$$J^{dark} \rightarrow 0$$

This is very important assumption and referred as 'dark channel prior'. The low intensity of dark channels is attributed mainly due to following three factors:

a. Images shadow includes low intensity values, e.g. shadows of trees, buildings and other objects in a scene.
b. Saturated color objects in a image have very low intensity value in other two bands of the RGB space, e.g. a deep blue sea may have very low values in green and red whereas high value in red.
c. Dark surfaces and objects exhibits low value as other color are more vivid like dark trunk of a tree in a bright sunny scene.

These observations have been verified statistically by studying over 5,000 dark channels, it revealed that 75 % of pixels in dark channel of an image have values close to zero whereas 90 % intensity values lies in range below intensity level 25. Figure 4.2 shows statistics of dark channel.

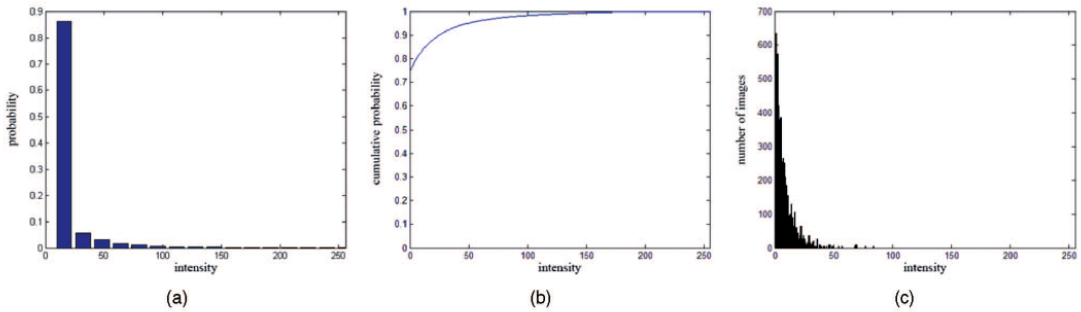

Figure 4.2 Dark channel statistics a: Histogram of 50,000 haze free dark channels b: Commutative Distribution c: histogram of the average intensity of each dark channel

4.2 Problem Definition

Fog has attenuates the input image, let J(x) is input image, I(x) is foggy image, t(x) is the transmission of the medium which is estimation of the light that is not scattered and reaches the camera. The attenuation of image due to fog can be expressed as:

$$I_{att}(x)=J(x)t(x) \qquad (4.1)$$

In case of homogeneous atmosphere transmission t(x) is represented as:

$$t(x) = e^{-\beta dx} \qquad (4.2)$$

here β is the scattering co-efficient and d(x) is the depth of the scene. Equation 4.2 describes an exponentially decaying function with depth and its rate is determined by the scattering coefficient. The second effect of fog is Atmospheric light effect and it is expressed as:

$$I_{Atmospheric\ light}(x)=J(x)(1 - t(x)) \qquad (4.3)$$

Atmospheric light effect is result of light scattering due to presence of floating water droplets of fog in the atmosphere. Atmospheric light effects causes shift in colors of the scene. As fogy image is combination of attenuation and Atmospheric light effect, therefore fogy image I(x) is given as:

$$I(x)= J(x)t(x) + A(1- t(x) \qquad (4.4)$$

The vector representation of fogy image model is as shown in Figure 4.3

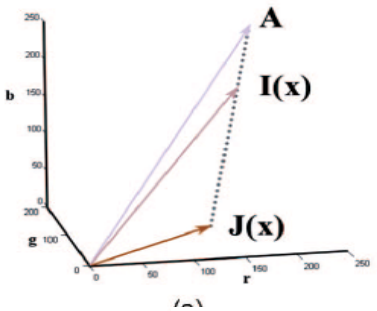

Figure: 4.3 Vector Representation of Hazy Image in RGB Space

In RGB space vector A, I(x) and J(x) are coplanar with their end point collinear in nature. The vector diagram also shows that a good estimation of A in RGB space will result in good restored value of J(x). Moreover, a shift in A in RGB space will also shift in J(x) in RGB space. Transmission can also be estimated from this vector diagram as a ratio between two line segments as:

$$t(x) = \frac{\|A - I(x)\|}{\|A - J(x)\|} = \frac{A^C - I^C(x)}{A^C - J^C(x)} \tag{4.5}$$

4.3 Transmission Estimation

After dark channel prior, we need to estimate transmission t(x) for proceeding further with the solution. Another assumption needed is that let Atmospheric light A is also known. We normalize equation 4.4 by dividing both sides by A:

$$\frac{I^c(x)}{A^c} = t(x)\frac{J^c(x)}{A^c} + 1 - t(x) \tag{4.6}$$

We are dealing with color images so need to normalize each color channel independently. As for most of the images depth does not change very abruptly and it can be taken as constant over a small portion. This assumption has limitations for edges in the images. Let Ω(x) is a small patch over which transmission remains constant. We apply the dark channel on both sides of above equation

$$\min_{y \in \Omega(x)} \left(\min_{C \in \{r,g,b\}} \frac{I^c(y)}{A^c} \right) = t(x) \min_{y \in \Omega(x)} \left(\min_{C \in \{r,g,b\}} \frac{J^c(y)}{A^c} \right) + 1 - t(x) \tag{4.7}$$

As already assumed t(x) is constant over small patch, so t(x) can be kept out of minimum operator. J(x) is image free from fog so it has value approximately zero :

$$J^{dark}(x) = \min_{y \in \Omega(x)} \left(\min_{C \in \{r,g,b\}} J^C(y) \right) = 0 \tag{4.8}$$

This yields the result in:

$$\min_{y \in \Omega(x)} \left(\min_{C \in \{r,g,b\}} \frac{J^C(y)}{A^C} \right) = 0 \tag{4.9}$$

Manipulating equation 4.8, 4.9 and equation 4.7 can be used to find t(x)

$$t(x) = 1 - \min_{y \in \Omega(x)} \left(\min_{C \in \{r,g,b\}} \frac{I^c(y)}{A^c} \right) \tag{4.10}$$

The term on the right side of equation 4.10 is dark channel of a normalised image; it provides an estimation of the transmission of the light from the scene point. Although dark channel provides good estimation for most of the images but for sky regions it is not a good approximation. Fog color is very similar to the color tone of the sky, this similarity is of great importance and helps in approximation of Atmospheric light. Sky region is theoretically at infinite distance; hence we can foresee almost no portion of light coming from infinite distant sky. Applying this analogy to equation 4.10 we can evaluate, for sky region the transmission as:

$$t(x)_{sky\_region} \longrightarrow 1$$

Fog is not a bad constituent always, in images fog gives us the feeling of depth and if we remove it absolutely from scene, images looks unnatural. In atmosphere even on clear day sky always has some moisture content which leads to some amount of light scattering. Hence clear day images also have some minor potion of fog, it is termed as 'Aerial Prospective'. To cater for this phenomenon a variable w is introduced in the equation 4.10 and gives:

$$t(x) = 1 - w \min_{y \in \Omega(x)} \left(\min_{C \in \{r,g,b\}} \frac{I^c(y)}{A^c} \right) \tag{4.11}$$

Value of w is application dependent and it lies between 0 and 1. As fog depends on depth of the image, using this method, more fog can be retained for depth elements.

A matlab implementation result of an input fogy image, its dark channel, transmission map and corresponding histogram are shown in Figure 4.4.

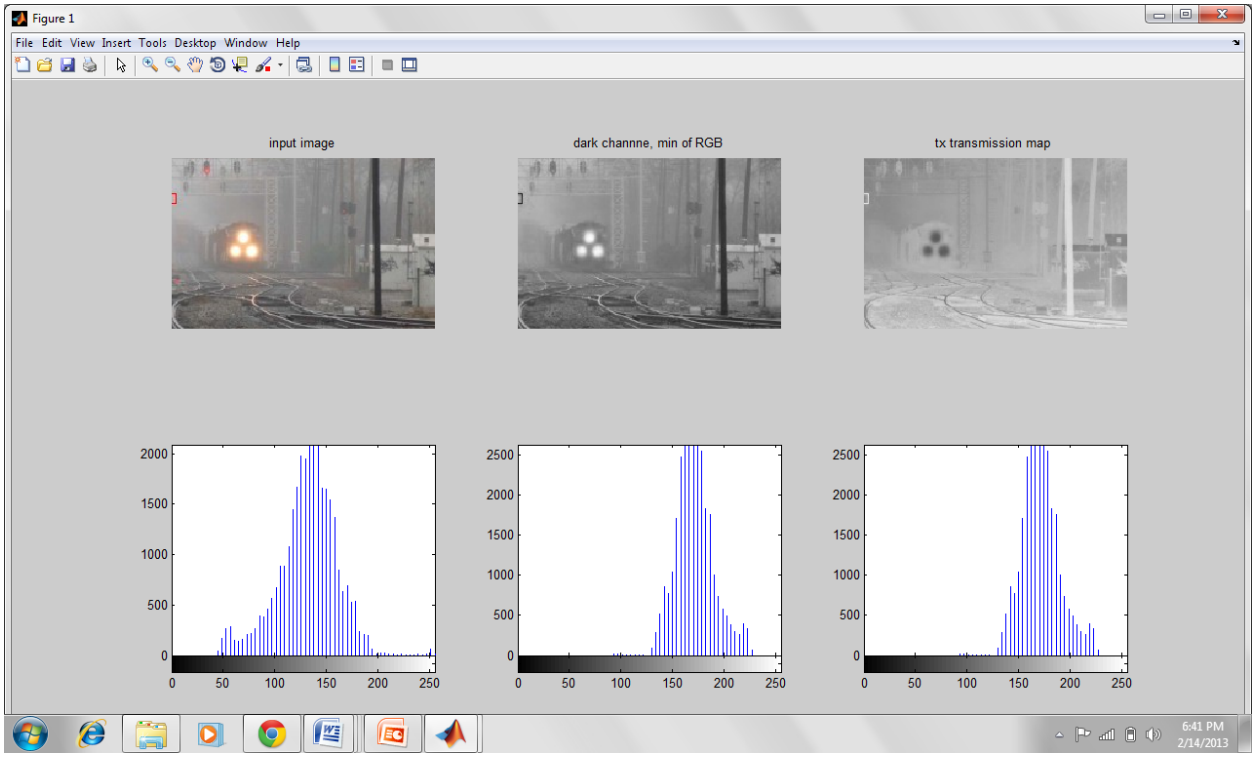

Figure 4.4: Input Foggy Image, Dark Channel, Transmission and Corresponding Histograms

4.4 Approximation of Atmospheric Light

Atmospheric light estimation is sensitive to correct color restoration of the images, Figure 4.3 illustrates the importance of good estimation of A. A wrong estimation will shift the recovered image J in RGB plane resulting in relative shifts in colors. Atmospheric light value is approximated from the image potion containing denser area in the fog, where fog concentration is maximum. Tan [] work is based on the brightest intensity pixel values in the image, it approximates A from the most haze denser area which contains brightest pixels. This method does not work when strong sunlight exists. In such cases wrong estimation of A from scene elements results in poor estimation of original colors. The error is due to brightest portion of image, may be a white object taken as fog for the correction of fogy image.

The method used utilizes the dark channel of the input image and takes its 10 percent of maximum intensity values and then take their max value as for value of Atmospheric light. The block process has been has shown as flow diagram.

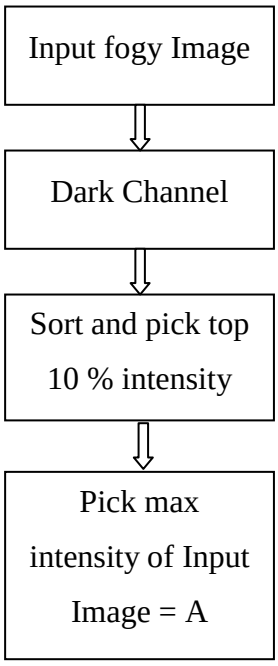

The Figure 4.5 gives a graphical representation of above block algorithm for estimation of Atmospheric light value from most haze opaque region.

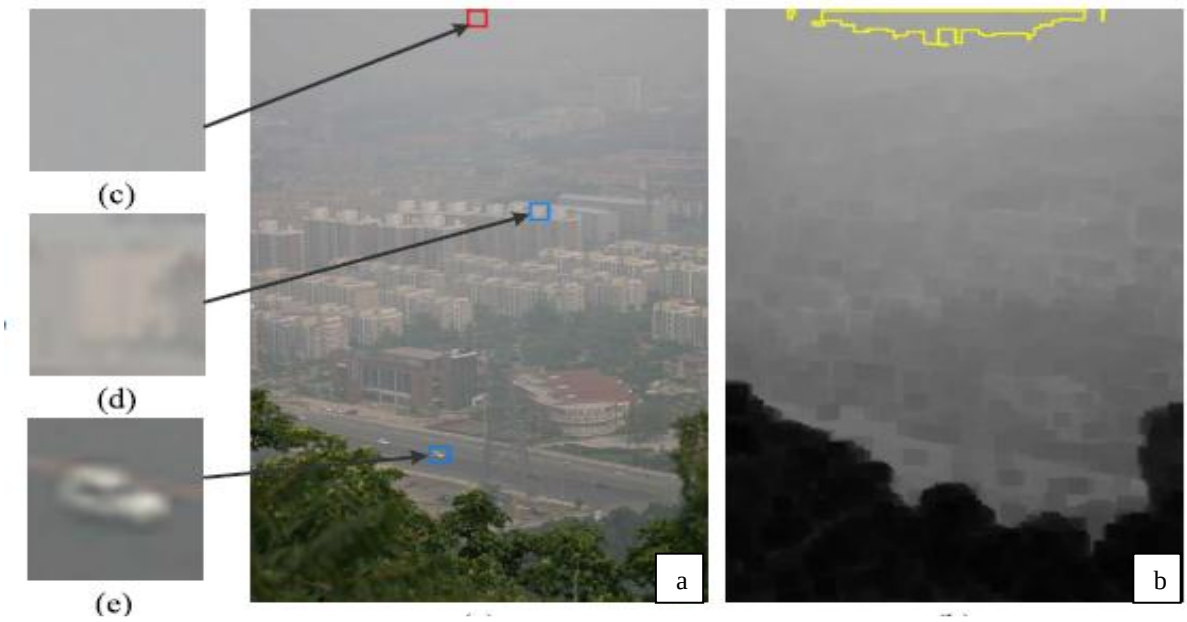

Figure 4.6 Estimation of Atmospheric light a: Fogy Image b: Dark channel c: Airlight Value d:, e: value>

4.4.1 Improvement in Estimation of Atmospheric Light

The method works fine for most of the fogy images and gives good estimation of value of A. However in some cases it fails and picks value of A from scene elements with images having multiple light sources and using small min filter. If window size of 15x155 is used then it estimates value of A from light source of the image. Some of the cases where it fails and picks value from scene elements instead of most haze opaque are shown in Figure 4.7.

Figure : 4.7 Atmospheric Light Value Estimation with Multiple Light Sources

An improved in the method has been proposed as to truncate the upper values so that maximum values which are picked from the scene portion rather than most haze opaque are negated. The proposed method is as under:

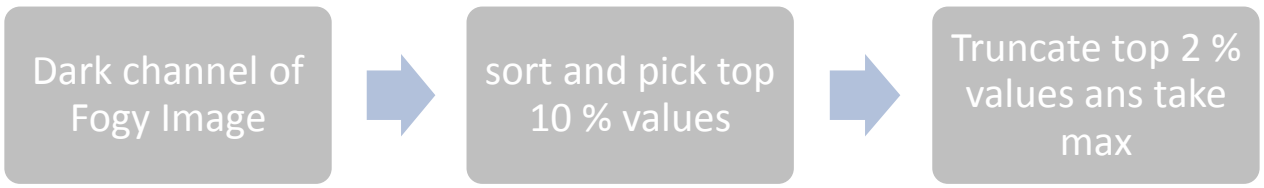

4.5 Restoration of Input Image

After implementing dark channel prior, Estimation of transmission map and Atmospheric light, haze free image can be restored using:

$$J(x) = \frac{I\ (x) - A}{\max(\ t(x), to)} + A \qquad (4.10)$$

In equation 4.10 t(x) has been bounded by a lower threshold t_0 as it is prone to noise and if it approaches to zero, can derive the equation to undefined domain. After experimentation and observations, value of has been fixed to 0.1 for most of the cases but if it is improved for denser fogy images up to 0.3 can improve the results.

4.6 Sensitivity Control of Model for Improved Results

Dark channel prior method is base on the fogy image model

$$I(x) = J(x)t(x) + A(1-t(x))$$

It can be interpreted as:

$$J(x) = \frac{I\ (x)}{t(x)} - A\left[\frac{1-t(x)}{t(x)}\right] \qquad (4.11)$$

and can be further simplified as

$$J(x) = \frac{I\ (x)}{t(x)} - A\left[\frac{1}{t(x)} - 1\right] \qquad (4.12)$$

The model is very sensitive to value of t(x) and subtracts from input image matrix for small values of t(x) which comes from very far distant scene contents. Intensity component also shoots up and cause oversaturation of recovered image. To control the sensitivity of the model we introduce another coefficient ϕ and equation 4.12 becomes:

$$I(x) = J(x)t(x) + A(1-\Phi t(x)) \qquad (4.13)$$

$$J(x) = \frac{I(\mathrm{x})}{\mathrm{t(x)}} - \mathrm{A}\left[\frac{1}{\Phi t(x)} - 1\right] \tag{4.14}$$

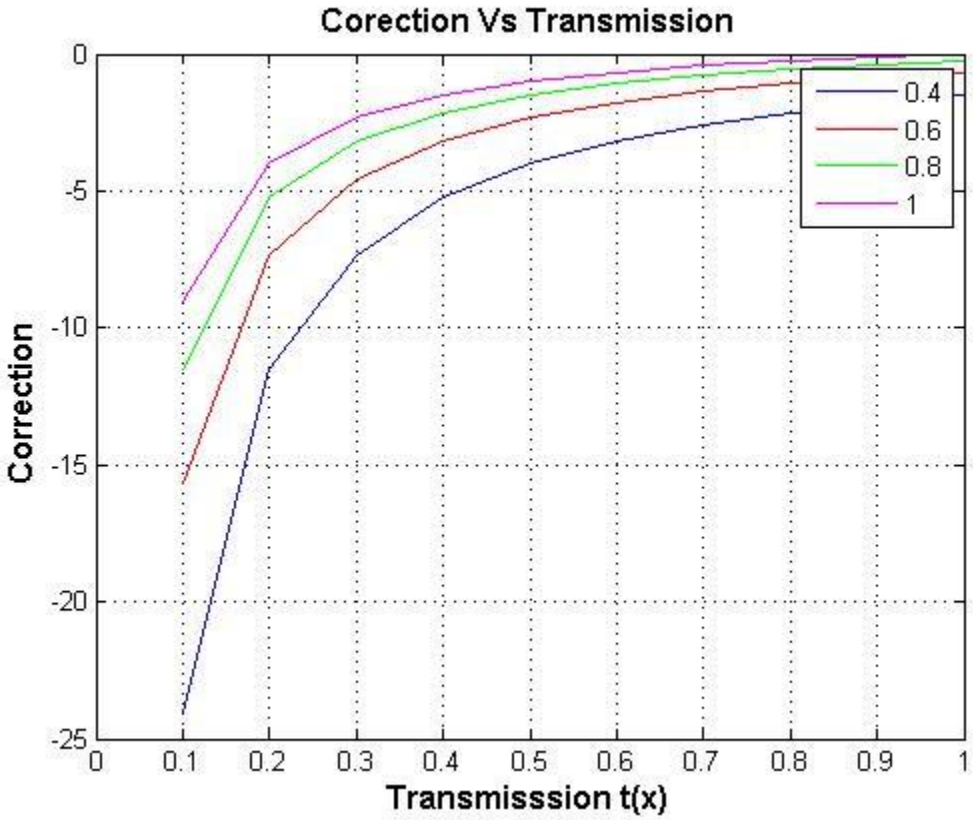

Figure: 4.8 Sensitivity Control of Model

Chapter 5

Results and Discussion

5.1 Classical Image Enhancement Techniques

Image enhancement and restoration techniques are based on the assumption that image and viewer are in a transparent medium. When these methods are applied to fogy images, results are not satisfactory as these do not consider depth of image. On the other hand, fogy images are degraded in proportion to the depth of the scene. Image intensity is degraded whereas Airlight is enhanced proportion to the depth of the element.

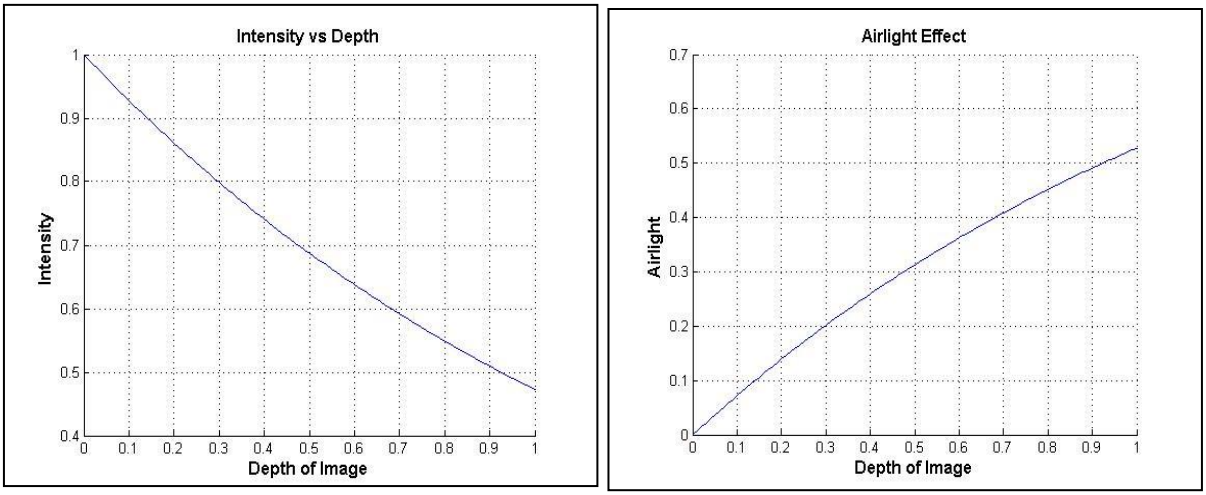

Figure: 5.1 Intensity and Airlight Variation with Image Depth

Light is scattered as it passes through water droplets suspended in the air. Intensity of the image decreases as less amount of light reaches the camera. The Airlight effect increases as an additive component is added in proportion to the distance from the scene point. Classical image enhancement techniques fail to remove scattering of light effect from the image, it rather further degrades in many of the cases. Due to enhanced light in the foggy image due to Airlight effect,

processing without treating degradation results in saturation of image. Histogram techniques have been utilised in pre-processing and post processing by some researchers, however, histogram equalization and histogram matching does not prove effective as depth of image is not involved. Figure 5.2 shows result of classical technique on fogy images.

Figure 5.2 Foggy Image and Classical Image Enhancement, Histogram Equalization and Average Filter

Figure: 5.3 Gaussian and Median Filter Application on Foggy Image

5.2 Atmospheric Light Effect

Image restoration from fogy image is dependent on value of Atmospheric light, a good estimation result in better approximation of transmission map. Tan [] method assumes that it is globally constant and can be approximated from the pixels which have the highest intensity values. It is based on the assumption that these are intensity values of the scene portion which have reached camera after undergoing scattering effects. Sun light is ignored in this assumption as in practical scenario it will have definite effects. The effect of Atmospheric light estimation is graphically illustrated in Figure 5.1

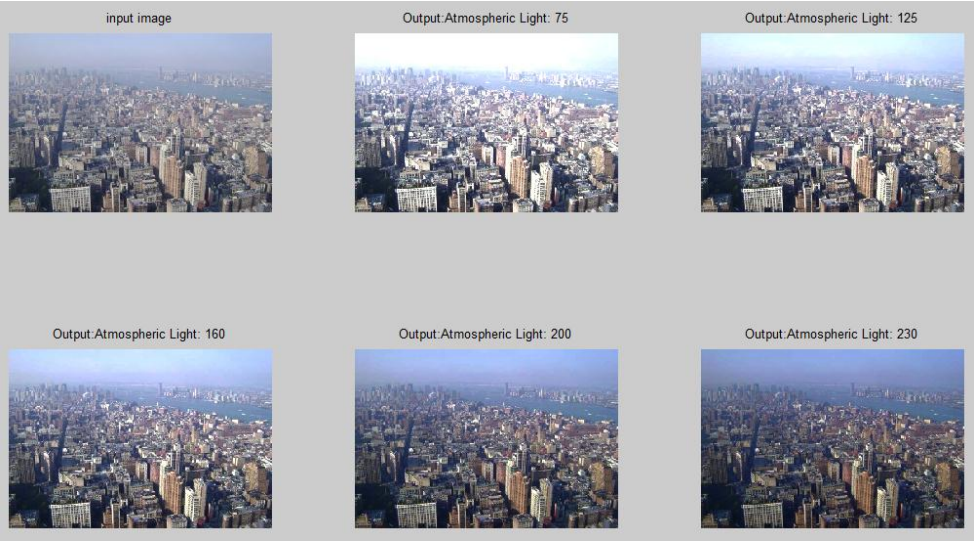

Figure: 5.4 Effect of Atmospheric light value – Normal Fog

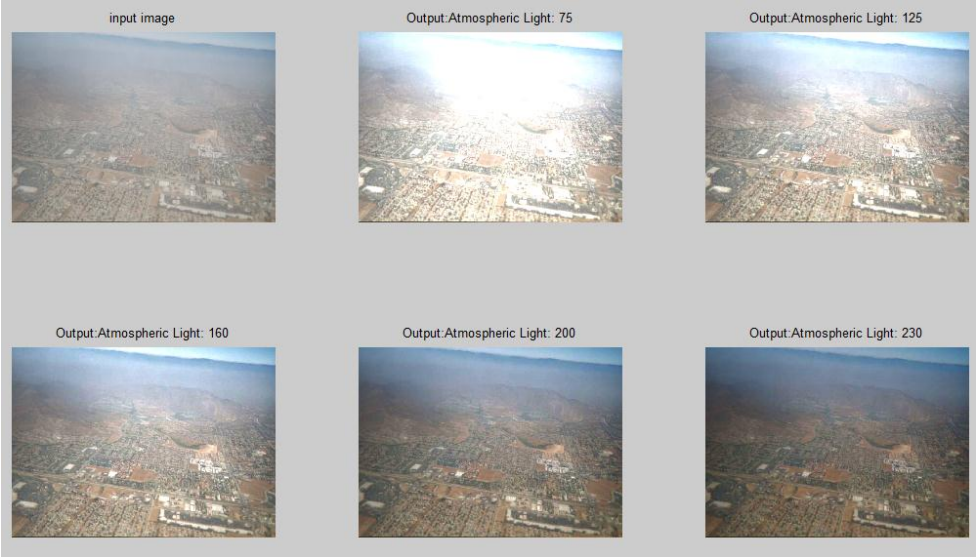

Figure: 5.5 Atmospheric light Effect – Dense Fog

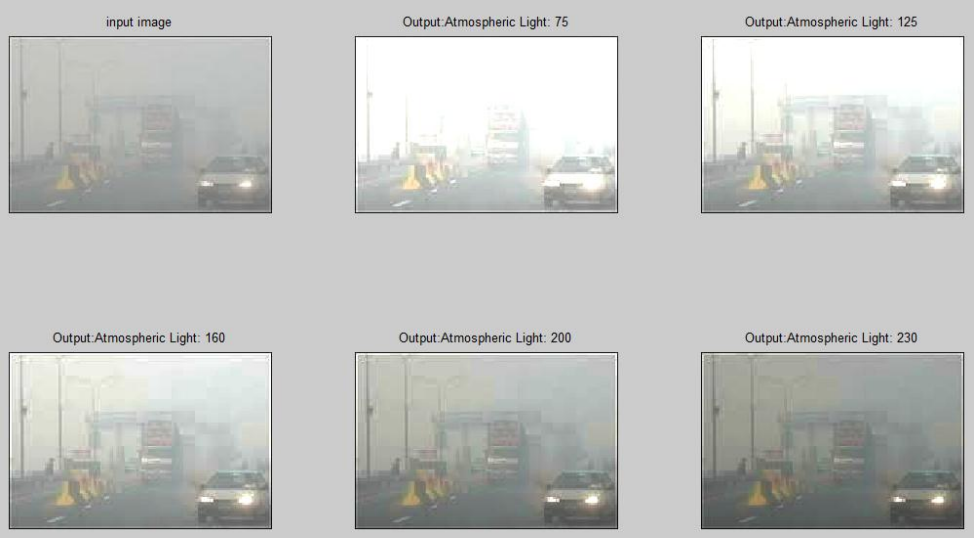

Figure: 5.6 Atmospheric light Effect – Thick Fog

5.3 Result with Improved Atmospheric light

The value of A is critical for restoration of haze free image, an under estimated value leads to saturation of output image and an over estimation results in darker image. It is to be estimated from the most haze opaque region of the dark channel of input image. The method purposed by Kaiming He[] take image portion as atmospheric light, therefore an upper clipping of Atmospheric value results in better contrast image. The results of image restoration with improved value of A are shown in Figure 5.7 -5.9.

Figure 5.7 Image Restoration with Improved Atmospheric Light Value – Dense Fog

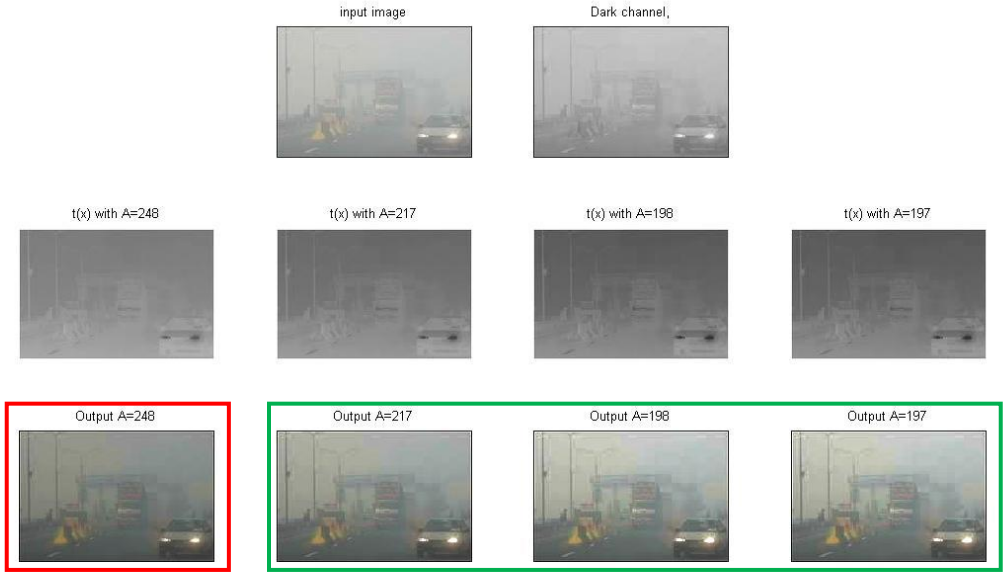

Figure 5.8 Image Restoration with Improved Atmospheric Light Value – Dense Fog

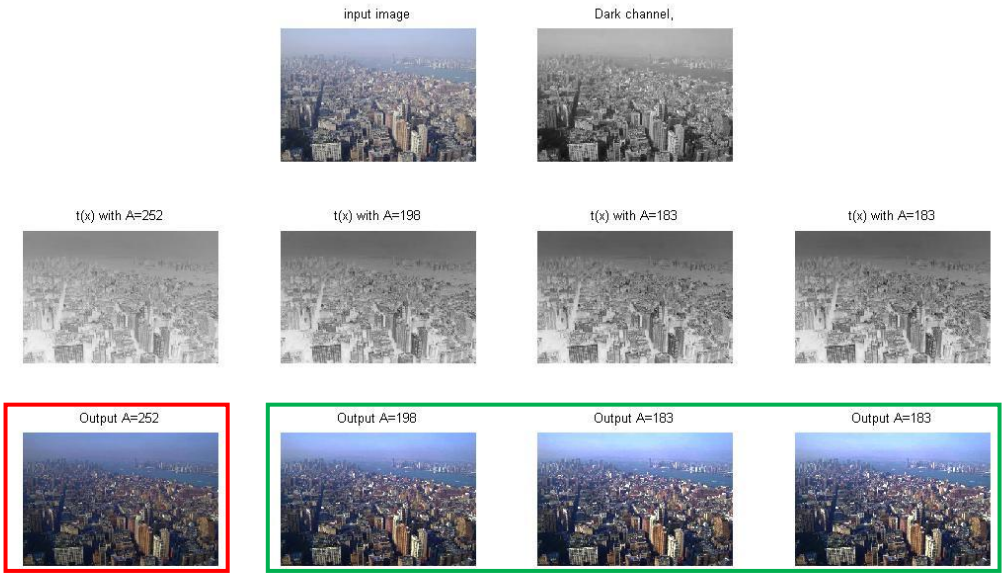

Figure 5.9 Image Restoration with Improved Atmospheric Light Value – Medium Fog

5.4 Results with Sensitivity Control of Fog Model

The fog model consists of two constituents' intensity attenuation and Airlight accumulation; both elements are proportional to the image depth. The sensitivity of both elements is different as one being an additive element and second being a multiplicative in nature. Result can be further enhanced by controlling coefficient Φ as illustrated by succeeding Figure 5.10 – 5.14.

Figure 5.10 Image Restoration with Sensitivity Control

Figure 5.11 Image Restoration with Sensitivity Control

Figure 5.12 Image Restoration with Sensitivity Control

Figure 5.13 Image Restoration with Sensitivity Control

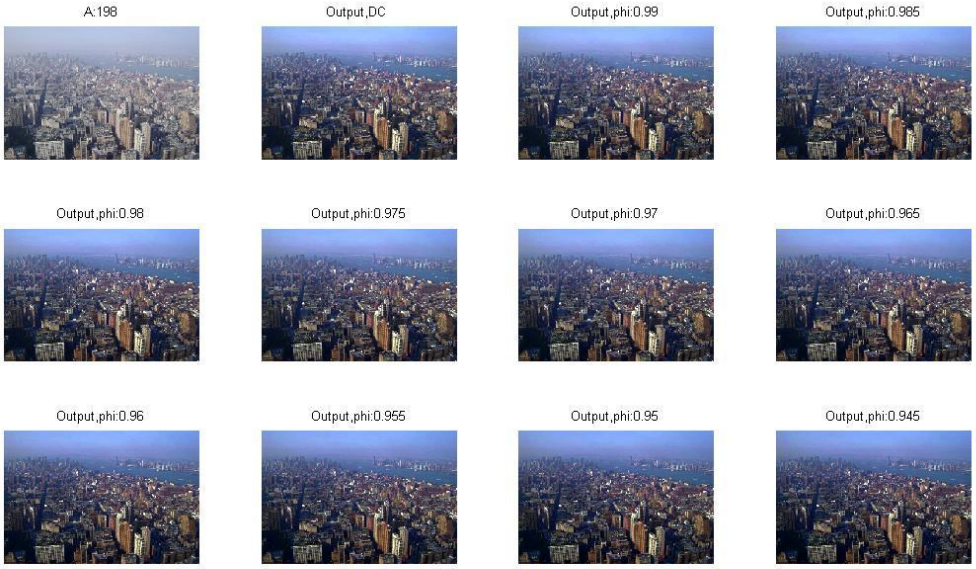

Figure 5.14 Image Restoration with Sensitivity Control

5.5 Conclusion and Future Scope

Single image dehazing has a lot of applications due to increasing dependence on surveillance and tracking systems vis-à-vis autonomous system demands. It is an under constraint problem with basing input from single image. Results can be further improved by improving image depth information. Further research can be directed towards developing hardware for driver assistance system for highway and motorway drivers. Similar customised hardware can be developed for commercial airlines pilot for landing and taking off during foggy weather.

APPENDIX - A

CLASSICAL IMGAE ENHANCEMENT TECHNIQUES ON FOGY IMAGE (MATLAB CODES)

```
%Classical Image Enhancement application on Fogy Images
% ehsanullah ehsan555@gmail.com
 clc;
 clear all;
 close all;
I=imread('E:/images/my7.jpg');
%% Histogram Equalization
for i=1:3
Ihe(:,:,i)=histeq(I(:,:,i)); % histogram equalization of RGB
end
Ihe1=cat(3,Ihe(:,:,1),Ihe(:,:,2),Ihe(:,:,3));
set(gcf,'outerposition',get(0,'screensize'));
subplot(221);
imshow(I);
title('Input Image','fontsize',12,'fontweight','b')
subplot(222);
imshow(Ihe1);title('Histogram Equalization','fontsize',12,'fontweight','b')
%% Average Filter
 J = fspecial('average',[3 3]); % average filter
for i=1:3
av(:,:,i)=imfilter(I(:,:,i),J);

end
avf=cat(3,av(:,:,1),av(:,:,2),av(:,:,3));

subplot(223);
imshow(avf);
title('Average Filter 3x3','fontsize',12,'fontweight','b');

 J = fspecial('average',[7 7]); % average filter
for i=1:3
av(:,:,i)=imfilter(I(:,:,i),J);

end
avf=cat(3,av(:,:,1),av(:,:,2),av(:,:,3));

subplot(224);
imshow(avf);
title('Average Filter 7x7','fontsize',12,'fontweight','b');


%% Gausian Filter
gf=fspecial('gaussian',[9 9]);
for i=1:3
gfl(:,:,i)=imfilter(I(:,:,i),gf);
```

```
end
gflt=cat(3,gfl(:,:,1),gfl(:,:,2),gfl(:,:,3));
figure(2)
set(gcf,'outerposition',get(0,'screensize'));
subplot(221);
imshow(I);
title('Input','fontsize',12,'fontweight','b');

subplot(222);
imshow(gflt);
title('Gausian Filter 9x9','fontsize',12,'fontweight','b');

%%  Min Filter
 for i=1:3
%gfl(:,:,i)=imfilter(I(:,:,i),gf);
mnf(:,:,i)=ordfilt2(I(:,:,i),1,ones(3));

end
mnfl=cat(3,mnf(:,:,1),mnf(:,:,2),mnf(:,:,3));
figure(2)
set(gcf,'outerposition',get(0,'screensize'));
subplot(223);
imshow(mnfl,[]);
title('Min Filter 3x3','fontsize',12,'fontweight','b');
%% Median Filter

for i=1:3
%im12=medfilt2(im1(:,:,2),[3 3]);
mdf(:,:,i)=medfilt2(I(:,:,i),[3 3]);

end
mdfl=cat(3,mdf(:,:,1),mdf(:,:,2),mdf(:,:,3));
subplot(223);
imshow(mdfl);
title('Median Filter 9x9','fontsize',12,'fontweight','b');

for i=1:3

mdf(:,:,i)=medfilt2(I(:,:,i),[9 9]);

end
mdfl=cat(3,mdf(:,:,1),mdf(:,:,2),mdf(:,:,3));
subplot(224);
imshow(mdfl);
title('Median Filter 9x9','fontsize',12,'fontweight','b');
```

APPENDIX – B

DARK CHANNEL FUNCTIONS

```
function J = dark_channel(I, patch_size)
% function J = dark_channel(I, patch_size);

% Computes the "Dark Channel" of corresponding RGB image.
% -Finds from the input image the minimum value among all
%  pixels within the patch centered around the location of the
%  target pixel in the newly created dark channel image 'J'
%  J is a 2-D image (grayscale).

% Example: J = dark_channel(I, 15); % computes using 15x15 patch

% Check to see that the input is a color image
if ndims(I) == 3
    [M N C] = size(I);
    J = zeros(M, N); % Create empty matrix for J
else
    error('Sorry, dark_channel supports only RGB images');
end

% Test if patch size has odd number
if ~mod(numel(patch_size),2)
    error('Invalid Patch Size: Only odd number sized patch supported.');
end

% pad original image
I = padarray(I, [floor(patch_size./2) floor(patch_size./2)], 'symmetric');

% Compute the dark channel
for m = 1:M
        for n = 1:N
            patch = I(m:(m+patch_size-1), n:(n+patch_size-1),:);
            J(m,n) = min(patch(:));
        end
end
end
```

TRANSMISSION FUNCTION

```
function [tc Abig] = trans(I, w)
% function [tc Abig] = trans(I);

% Computes the coarse transmission map 'tc' of input image I
% - uses patch size of 3
% Also computes estimation of atmospheric light, Abig
% Abig is an MxNx3 image, where all values in each color plane
% are the same value estimation of the atmospheric light for that color.

% tc(x) = 1 - w * min (I/Ac)
%    - tc(x) is 1 - minimum of pixels in patch centered around x of
%          input image normalized by calculated atmospheric light

% w sets the amount of haze preserved, range = 0 to 1;
%   - amount of haze is inversely proportional to w
%   - i.e. w = 0.95 preserves 5% of the haze

% Example: [tc Abig] = trans(I, 0.95);
%   Computes the coarse transmission map and atmospheric light of input
%   image I, preserving 5% of image haze.



w = max(min(w,1),0); % Make sure w is between 0 and 1.
I = double(I); % Make sure input image is double precision
vert_size = size(I,1); %IÍ¼ÏñµÄµÚÒ»Î¬´óÐ¡£¬¼´yÖá´óÐ¡
horiz_size = size(I,2);%

% Compute the Dark Channel of image I using a patch size of 15x15
Jdark = dark_channel(I, 1);
```

```
% Estimate Airlight of image I
   % Compute number for .1% brightest pixels
   n_bright = ceil(0.001*vert_size*horiz_size);
   % Loc contains the location of the sorted pixels
   [Y,Loc] = sort(Jdark(:));

   %column-stacked version of I
   Ics = reshape(I, vert_size*horiz_size, 1, 3);

   %init a matrix to store candidate airlight pixels
   Acand = zeros(n_bright,1,3);
   %init matrix to store largest norm airlight
   Amag = zeros(n_bright,1);

   % Compute magnitudes of RGB vectors of A
   for i = 1:n_bright
     Acand(i,1,:) = Ics(Loc(vert_size*horiz_size+1-i),1,:);%È¡»Ò¶ÈÖµ×î´óµÄ¼¸öµã
     Amag(i) = norm(Acand(i,:)); %normÎªÇóÆä·¶Êý£¬´Ë¡Ä¬ÈÏ¾ÍÊÇ¾ÍÆä¾ØÕó×î´óÖµÔªËØ
   end

   % Sort A magnitudes
   [Y2,Loc2] = sort(Amag(:));
   % A now stores the best estimate of the airlight
   A = Acand(Loc2(n_bright-19:n_bright),:);
   % finds the max of the 20 brightest pixels in original image
   A = max(A);

% Expand A to size of input image
Abig = zeros(vert_size, horiz_size, 3);
Abig(:,:,1) = A(1);
Abig(:,:,2) = A(2);
Abig(:,:,3) = A(3);
```

```
% Compute the 'dark channel' of the normalized input image with a 15x15
% patch
Jdark_norm = dark_channel(I./Abig, 1);

% Compute coarse transmission map
tc = 1 - w*Jdark_norm;

end
```

FUNCTION HAZE FREE

```
function J1 = hazefree(I, tc, A)
% function J = hazefree(I, t, A);
% Computes a haze free image
% default lower bound for transmission is 0.1
%   I - Original image - Double precision with range 0 to 1
%   t - Transmission Map estimate - Can be a coarse or fine estimate
%   A - Atmospheric light - MxNx3

tmin = 0.1; % Lower bound for transmission map

% Create empty matrix for dehazed image
J1 = zeros(size(I));

% Compute each dehazed color channel using haze formation equation
for c = 1:3

   J1(:,:,c) = (I(:,:,c) - A(:,:,c))./(max(tc, tmin)) + A(:,:,c);

end
```

FUNCTION MATING LAPLACIAN

```
function L = matLap(I)
% L = matLap(I)
% Computes the "Matting Laplacian" matrix for image I with a window size
% of 3x3 (default). To adjust window size, change parameter 'win_size'

% Run time is approximately 70 seconds for 400x600 image on
% AMD Turion Neo x2 processor with 4GB RAM

win_size = 3; % Set window size to 3x3
win_els = win_size.^2; % calculate number of window elements
l_els = win_els.^2; %# of elements calculated in each forloop iteration

% Calculate the size of the border of pixels not in matlap calculation
%   - For example, if win_size = 3x3, there is a 1 pixel border to avoid
%       around the whole image.
win_bord = floor(win_size./2);

% epsilon in Matting Laplacian equation. Levin et al. report using this
% value, but can be adjusted depending on image.
e = 0.000001;

[m,n,c] = size(I); % find number of rows, columns, and colors of I
numpix = m*n; % calculate number of rows or columns for L

k = reshape(1:numpix, m, n); % create matrix of indices for each pixel
U = eye(win_size); % create a an identity matrix of win_size
D = eye(win_els); % create an identity matrix of win_els

% calculate number of terms that will be created in for loop
num_els = l_els*(m-2*win_bord)*(n-2*win_bord);

% create empty index vectors for L
ind_i  = ones(1,num_els);
ind_j = ind_i;

% create empty vector to store calculated L terms
els = zeros(1,num_els);

% initialize counter for calculating where to deposit new index and L terms
count = 0;

% Begin Matting Laplacian term calculations!
for x = (1 + win_bord):(n - win_bord) % start and end within border
    for y = (1 + win_bord):(m - win_bord) %start and end within border

        % Extract (win_size x win_size) window from image and reshape to
        % (win_els x c) matrix
        wk = reshape(I(y-win_bord:y+win_bord,x-win_bord:x+win_bord,:),...
                win_els, c);
```

```
        % Extract pixel indices for window, reshape to (win_els x 1)
        w_ind = reshape(k(y-win_bord:y+win_bord,x-win_bord:x+win_bord),...
                1, win_els);

        % Create grid of L locations
        [i j] = meshgrid(w_ind, w_ind);
        % Reshape to vectors
        i = reshape(i,1,l_els);
        j = reshape(j,1,l_els);
        % Add locations to L index vectors
        ind_i((count*l_els + 1):(count*l_els+l_els)) = i;
        ind_j((count*l_els + 1):(count*l_els+l_els)) = j;

        win_mu = mean(wk)'; % Calculate mean of colors in window

        % Calculate normalized covariance matrix
        %  - direct calculation is slightly faster than using cov function
        win_cov = wk'*wk/win_els-win_mu*win_mu';

        % Calculate difference between window values and mean
        dif = wk' - repmat(win_mu,1,win_els);

        % Compute L terms
        % Note that both '\' and inv have been tried and don't result in
        % a noticeable time difference, likely due to the fact that the
        % matrix being inverted is very small. So inv was used for clarity.
        elements = D - (1 + dif(:,1:win_els)'*inv(...
            win_cov + e./win_els.*U)*dif(:,1:win_els))...
            ./win_els;
        % Add terms to L elements vector
        els((count*l_els + 1):(count*l_els+l_els)) = ...
            reshape(elements,1,l_els);

        % increment count index
        count = count + 1;
    end
end

% Compute final L matrix. Note that sparse automatically adds together
% terms sharing the same location.
L = sparse(ind_i, ind_j, els, numpix, numpix);
```

REFRENCES

A. Gijsejij and T. Gevers. Color constancy using natural image statistics. in proceeding of IEEE CVPR, 2007. 5

A. Levin, D. Lischinski, Y. Weiss, ”A Closed-Form Solution to Natural Image Matting,” IEEE Transactions on Pattern Analysis and Machine Intelligence, Vol. 30, No. 2, February 2008.

Chaudhury, K.N., Sage, D., and Unser, M.: ‘Fast O(1) bilateral filtering using trigonometric range kernels’, IEEE Trans. Image Process., 2011, 20, (2), pp. 3376– 3382

D. J. Jobson, Zia-ur-Rahman, G. A. Woodell, “Properties and performance of a Center/Surround Retinex,” IEEE Transactions on Image Processing, vol. 6, no. 3, March 1997.

E. McCartney. Optics of the atmosphere: Scattering by molecules and particles. John Wiley and Son, 1975. 2

F. Cozman and E. Krotkov. Depth from scattering. In Proceedings of the 1997 Conference on Computer Vision and Pattern Recognition, vol. 31, pp. 801–806., 1997. 1, 2

H. Koschmieder, 1924, ”Theorie der horizontalen sichtwetie,” In Bietz. zur Phys. d. freien Atm., 171-181.

J. Kopf, B. Neubert, B. Chen, M. Cohen, D. Cohen-Or, O. Deussen, M . Uyttendaele, D. Lischinski, ”Deep photo: Model-based photograph enhancement and viewing,” ACM Transactions on Graphics(Proceedings of SIGGRAPH Asia 2008, Vol. 27, No. 5)

J. P. Tarel, N. Hautiere, ”Fast Visibility Restoration from a Single Color or Gray Level Image,”IEEE 12th International Conference on Computer Vision, 2009.

J. Tarel and N. Hauti, "Fast visibility restoration from a single color or gray level image," in Proc. 2009 IEEE International

K. He, J. Sun, X. Tang, ”Single Image Haze Removal Using Dark Channel Prior,”IEEE Transactions on Pattern Analysis and Machine Intelligence, Vol. 33, 2011.

Kopf, J., Neubert, B., Chen, B., Cohen, M., Cohen-Or, D., Deussen, O.,Uyttendaele, M., and Lischinski, D.: ‘Deep photo: model-based photograph enhancement and viewing’, ACM Trans. Graph., 2008, 27,

L. Kratz and K. Nishino, "Factorizing scene albedo and depth from a single foggy image," in Proc. 2009 IEEE International Conference on Computer Vision (ICCV).

N. Hautiere, J. Tarel, and D. Aubert. Toward fog-free in vechicle vision systems through contrast restoration. CVPR, 2007. 1

R. C. Gonzalez, R. E. Woods, “Digital Image Processing,” Third Edition, Pearson Publications.

R. Szeliski, R. Zabih, D. Scharstein, O. Veksler, V. Kol mogorov, A. Agarwala, M. Tappen, , and C. Rother. A comparative study of energy minimization methods for markov random fields. in proceeding of ECCV, 2006. 5

R. T. Tan, ”Visibility in Bad Weather from a Single Image,” IEEE Conference on Computer Vision and Pattern Recognition, CVPR 2008.

S. G. Narasimhan and S. K. Nayar. Contrast restoration of weather degraded images. IEEE PAMI, 25(6), June 2003. 1, 2

S. G. Narasimhan, S.K. Nayar, ”Vision and the Atmosphere,”International Journal of Computer Vision, 2002.

S. K. Nayar and S. G. Narasimhan. Vision in bad weather. In ICCV (2), pages 820–827, 1999. 1, 2

S. Narayanan, S. G. Narasimhan, ” Interactive deweathering of an image using physical models ,” Computer Vision, 1999

S. Narayanan, S. G. Narasimhan, ” Vision in Bad Weather,” Computer Vision, 1999

S. Shwartz, E. Namer, and Y. Schechner. Blind haze separation. CVPR, 2006. 1

V. Cardei, B. Funt and K. Barnd, "White point estimation for uncalibrated images," in Proc. 1999 IS&T/SID Seventh Color Imaging Conference, pp. 97-100.

Y. Schechner and N. Napel. Clear underwater vision. CVPR, 2004. 8

Y. Y. Schechner, S. G. Narasimhan, and S. K. Nayar. Instant dehazing of images using polarization. 1:325–332, 2001. 1, 2

Y. Y. Schechner, S. G. Narasimhan, S.K. Nayar, ”Instant Dehazing of Images using Polarisation,”Proceedings of Computer Vision and Pattern Recognition, Vol. 1, pp. 325-332, 2001.